WILEY | Hindawi

Research Article

Design Optimization of Feeding Networks with a Special Size for Self-Interference Cancellation

Xiaotian Huang [ID],[1] **Baohua Sun** [ID],[1] **Li Sun** [ID],[2] **Rui Zhang** [ID],[1] **Wei Niu** [ID],[1] **and Ruize Niu** [ID][1]

[1]*Key Laboratory of Antennas and Microwave Technology, Xidian University, No. 2 South Tai-Bai Road, Xi'an 710071, Shaanxi, China*
[2]*School of Microelectronics, Northwestern Polytechnical University, Xi'an 710072, China*

Correspondence should be addressed to Li Sun; lisun@nwpu.edu.cn

This letter introduces an effective self-interference cancellation (SIC) for improving isolation between transmit (Tx) ports and receive (Rx) ports of an in-band full-duplex antenna with feeding networks (FNs). A significant isolation improvement is realized by replacing the traditional FNs of the antenna with SICFNs. The coupling between Tx and Rx ports is canceled in the FNs due to the specific power ratios and phase difference. Though a Python optimization procedure, the optimal values of the key parameters of the SIC FNs can be determined. To validate the proposed SIC technique, the prototype consisting of two four-element antenna arrays and four SICFNs designed with the technique is fabricated. The results of measurements performed in an anechoic chamber show an isolation improvement of 15 dB at 3.6 GHz, while only 0.3 dB gain loss for the antenna array as a sacrifice is observed.

1. Introduction

In-band full-duplex (IBFD) technology is very attractive in wireless communication systems because it can double the spectrum efficiency compared with traditional time division duplexing (TDD) or frequency division duplexing (FDD) [1, 2]. One of the critical challenges in IBFD wireless communications is the cancellation or suppression of self-interference (SI). The SI is caused by its own transmit signal, which is much stronger than the desired received signal. In addition to using self-interference cancellation (SIC) techniques at the analog and digital stages [3–6], high isolation at the antenna stage is essential to avoid deterioration of the signal-to-noise ratio (SNR). In general, at least 80 dB isolation should be achieved at the antenna stage [7]. And higher isolation is of benefit to decrease the complexity and requirements of analog and digital stages.

The space division duplex (SDD) separates the receiving (Rx) antennas from the transmitting (Tx) antennas. So good isolation between them can be obtained. However, the spatial interference suppression alone is not enough to achieve sufficient isolation at the antenna stage, especially when the installation space of the antenna is limited by the environment, and the spacing between the Rx antennas and the Tx antennas is not large enough. The techniques for achieving higher isolation at the antenna stage can be classified into two main types: The first one is to suppress the coupling along the propagation path between antennas directly through decoupling techniques, such as electromagnetic band-gap (EBG) structures [8], slotted meander-line resonators [9], soft surface [10], interdigital lines [11], metamaterial [12], and defected ground structure (DGS) [13]. These structures occupy a certain amount of space, thus increasing the complexity of the antenna structure. Another solution achieves high isolation through coupling cancellation. For

TABLE 1: Comparison of currently proposed interference-reduction techniques.

| Reference number	Decoupling scheme	Form of the SIC FN	Self-interference symmetry	Occupy extra space
[8–13]	Block structures	—	—	Yes
[15–18]	Decoupling network	—	—	Yes
[20]	Decoupling superstrate	—	—	Yes
[21]	SIC FN	Differential feeding	Symmetry	No
[22, 23]	SIC FN	Pairwise antiphased feeding	Symmetry	No
[24]	SIC FN	Butler matrix beamforming networks	Symmetry	No
This letter	SIC FN	Customize the size according to the antenna	No limit	No
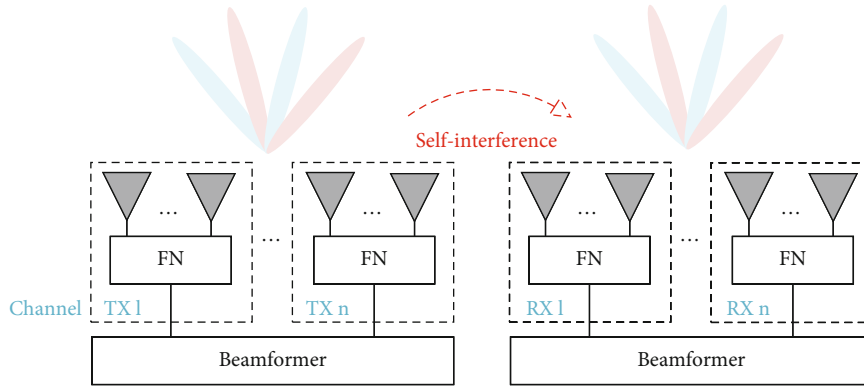
FIGURE 1: A SDD MIMO communication system.
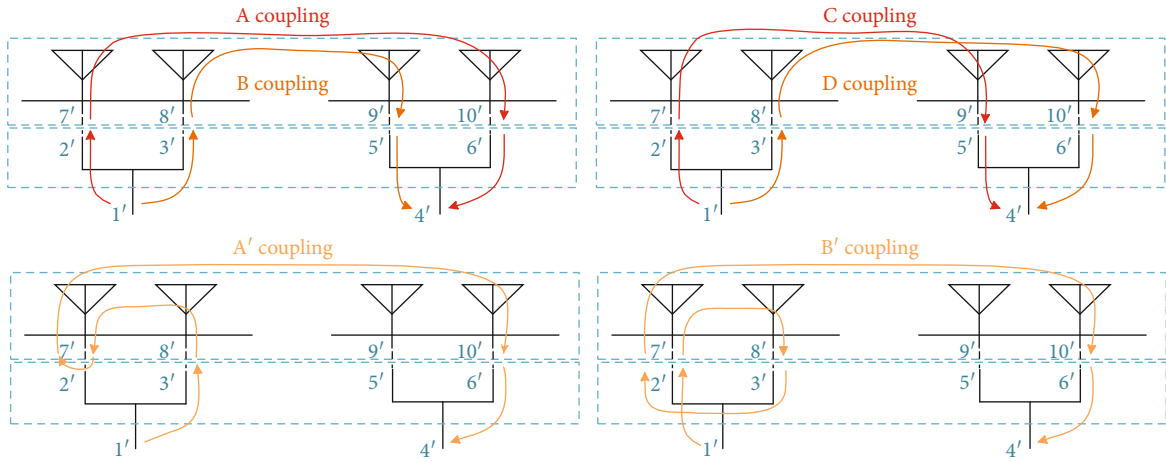
FIGURE 2: 2×2 antenna array with FNs.

example, reflective terminal [14], decoupling network [15–18], decoupling surface [19], and decoupling superstrate [20] are used to introduce additional coupling paths to cancel the coupling of the original propagation paths. Nevertheless, the complexity of the feed structures or the size of the antenna increased due to the additional coupling structures.

A feeding network (FN) can form a subarray with antennas to obtain higher gain, which can also be used simultaneously as a SIC FN. The coupling from one channel to another channel can be decomposed and merged again by the FNs. The rational design of the FNs can realize the cancellation of the coupling without introducing additional coupling. In [21], self-interference suppression was achieved by using differential feedings in an 8×8 antenna array, but Tx ports and Rx ports with different polarizations are necessary. In [22, 23], the FNs utilizing the pairwise antiphased feeding technique were used to improve the isolation between subarrays. Yet this technique can only be used to cancel the interference between different polarizations of the same array. The FNs that realized self-interference cancellation in [24]
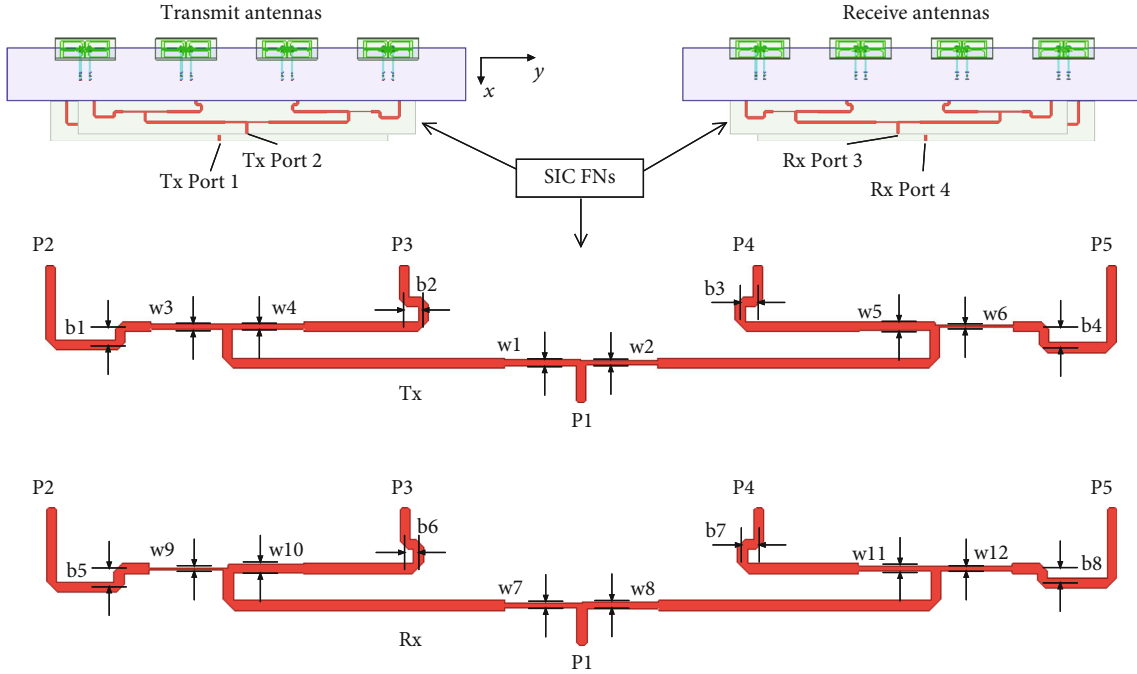
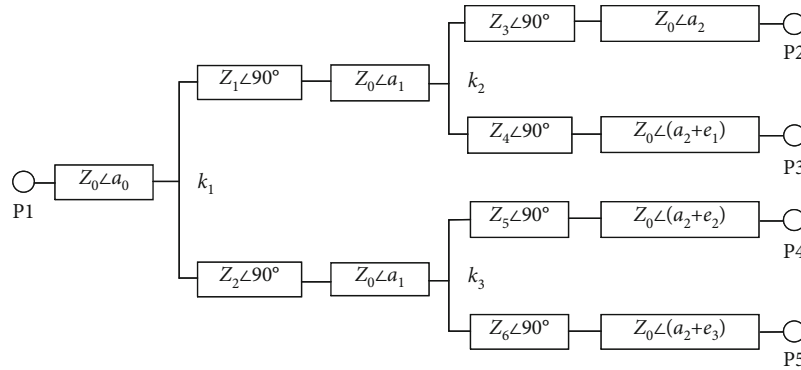FIGURE 3: Geometry of the antenna array and its FNs.

FIGURE 4: Topology of the SIC FNs.

also require the antenna to be symmetric at the center. To sum up, a comprehensive comparison of currently proposed interference-reduction techniques is given in Table 1.

The forms of the IBDF antenna array are varied, such as the array in the SDD MIMO system in Figure 1. Unlike the scenarios mentioned in the techniques above, the amplitude of the couplings between the antennas of the two channels are unequal, and the phase of the couplings are irregular, which will make the self-interference asymmetrical. In this scenario, a more general methodology to design the SIC FNs is proposed in this letter. FNs only composed of unequal power dividers are used as the design topology, and the isolation between the Tx and Rx ports is improved by 15 dB. The advantage of this topology is that it is simple enough to be placed in some compact arrays [25, 26].

This letter is organized as follows. The design process of the SICFNs is described in Section II. Section III presents the performances of the antenna array with the SIC FNs. Conclusions are drawn in Section IV.

2. Design of the SIC FNs

2.1. Theoretical Analysis of the SIC Technique. The theoretical analysis of the proposed SIC technique is based on the S-parameter matrix cascade calculation formula in [27], which is also used in the design of the FN in this paper.

As an illustrative example, a 2×2 antenna array is selected for coupling analysis, as depicted in Figure 2. The coupling coefficient $S_{1'4'}$ can be expressed by applying the formula in [27] to cascade the S-parameter matrix of the array and the FNs. And the expression can be simplified by omitting the higher-order terms as follows:

$$
\begin{aligned}
S_{1'4'} &\approx S_{1'2'} S_{7'10'} S_{4'6'} + S_{1'3'} S_{8'9'} S_{4'5'} + S_{1'2'} S_{7'9'} S_{4'5'} \\
&\quad + S_{1'3'} S_{8'10'} S_{4'6'} + S_{1'3'} S_{7'8'} S_{2'2'} S_{7'10'} S_{4'6'} \\
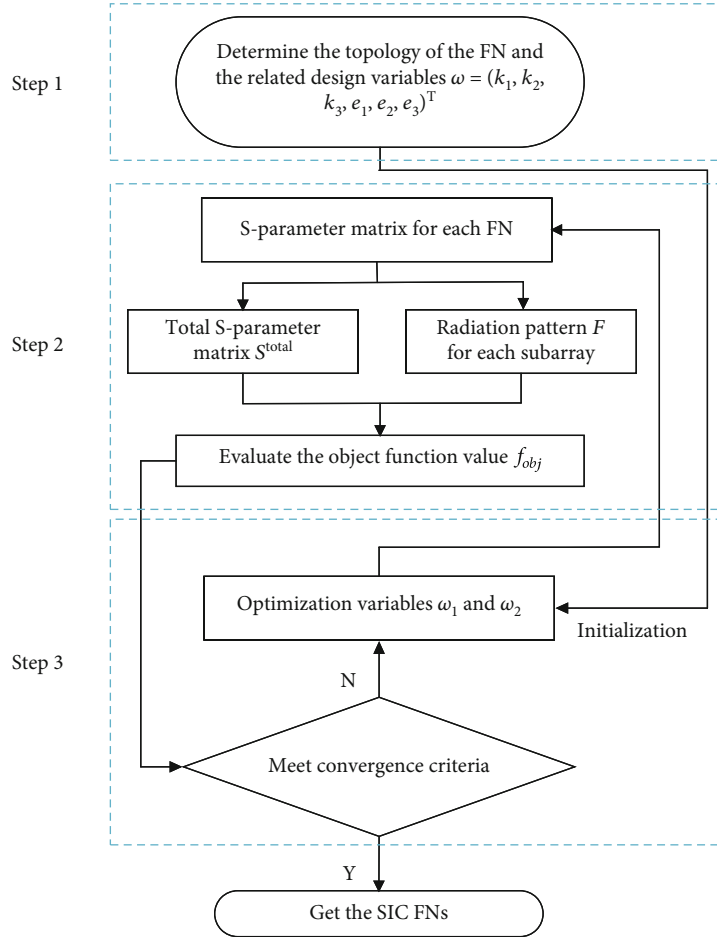&\quad - S_{1'2'} S_{7'8'} S_{2'3'} S_{7'10'} S_{4'6'} + \cdots.
\end{aligned}
\tag{1}
$$

Figure 5: Design flowchart of the SIC FNs.

Table 2: Design parameters of the SIC FNs.

	k_1	k_2	k_3	k_4	k_5	k_6
Optimized results	1.43	1.03	3.95	0.69	0.25	0.97
	e_1	e_2	e_3	e_4	e_5	e_6
	1.78	358.62	2.81	352.11	357.09	354.3
Dimensions (mm)	w1	w2	w3	w4	w5	w6
	1.05	0.74	0.92	0.87	1.38	0.3
	w7	w8	w9	w10	w11	w12
	0.73	1.05	0.3	1.38	0.87	0.92
	b1	b2	b3	b4	b5	b6
	3	3.2	2.9	3.5	3	2.2
	b7	b8				
	2.7	2.4				

The first four of these terms can be considered the four most direct couplings, already shown in Figure 2, marked A-D. The four couplings are the most critical couplings that affect $S_{1'4'}$.

The couplings represented by the fifth and sixth terms in (1) are also shown in Figure 2, marked A' and B'. Together with the omitted higher-order terms, they repre-sent the coupling of multiple transmissions and reflections through the internal loop formed by the antennas and the FNs.

Consequently, it is possible to design the SIC FN so that its S-parameter matrix meets the requirement of having $S_{1'4'} = 0$. Since calculating the coupling coefficient involves a large-scale matrix operation and the radiation performance
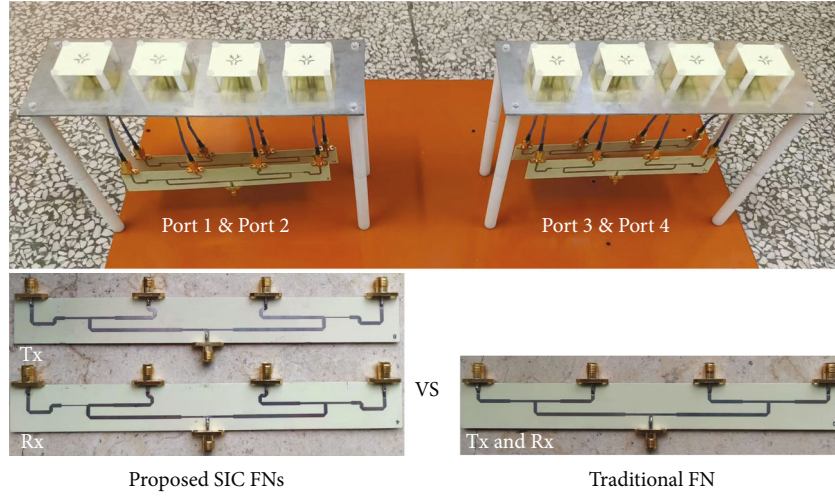
FIGURE 6: Fabricated antenna and FNs.
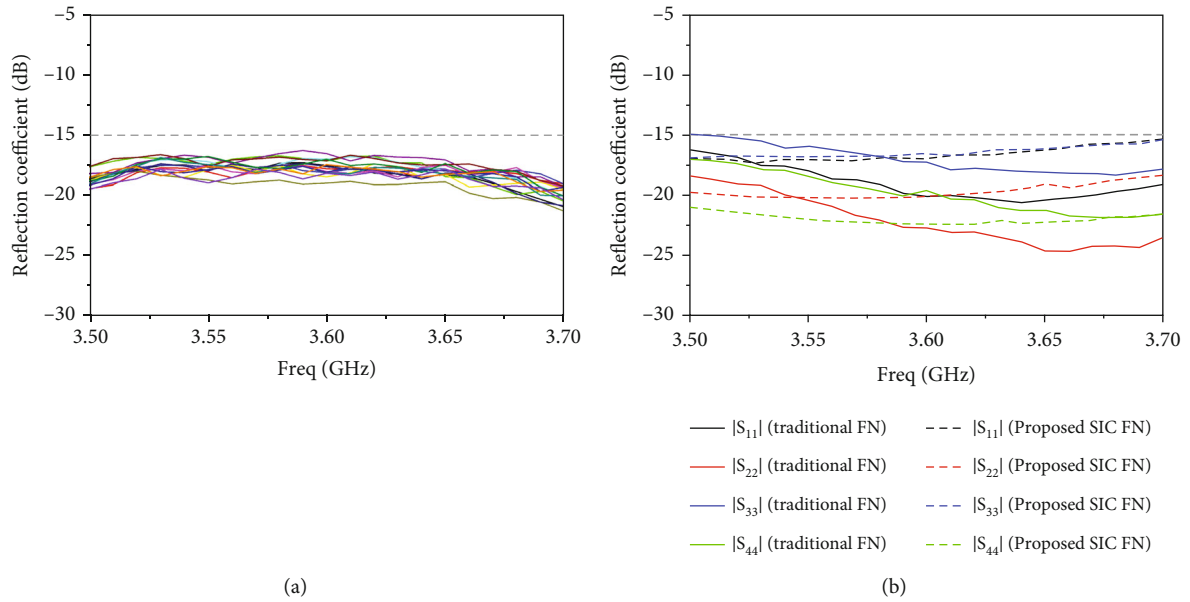

(a)

(b)

FIGURE 7: Measured reflection coefficients of the fabricated antenna. (a) Each antenna element. (b) Antenna with different FNs.

of each subarray should be considered, a Python optimization procedure is introduced based on the differential evolution algorithm (DE).

2.2. Design of the FNs Based on SIC Technology. To illustrate the effectiveness of the SIC technique, a design example of an antenna array with the SIC FNs is shown in Figure 3. The cross-dipole antenna reported in [28] is employed as the element of the array for our study, which works at 3.6 GHz. The element spacing is 58.3 mm ($\sim 0.7\lambda_{3.6}$, where $\lambda_{3.6}$ is the free-space wavelength at 3.6 GHz). In addition, an array spacing of 167 mm ($\sim 2\lambda_{3.6}$) is selected. The different polarized ports of the Tx antenna array and the Rx antenna array act as their respective channels.

The geometry of the FNs is shown in Figure 3. The FNs connected at different polarized ports of the antenna are

chosen to be the same due to the symmetry of the structure. To cancel the coupling under different paths in the FNs, the power ratios and phase differences of the FNs are the most critical factors. Considering the complexity of the design, the width of the quarter-wavelength impedance transformers, named w1-w12, and the length of the bend lines, named b1-b8, are used as design variables while keeping other parameters fixed.

The topology of the FNs in circuit form is given in Figure 4, which is used to realize the fast calculation of the S-parameter matrices of the SIC FNs in the optimization procedure. Z_1-Z_6 represent the impedance of the quarter-wavelength impedance transformers, and the power ratio k_1-k_3 is used to correlate them in pairs, which can reduce the optimization variables. For the same reason, the electrical length e_1-e_3 represent the phase differences. Therefore,
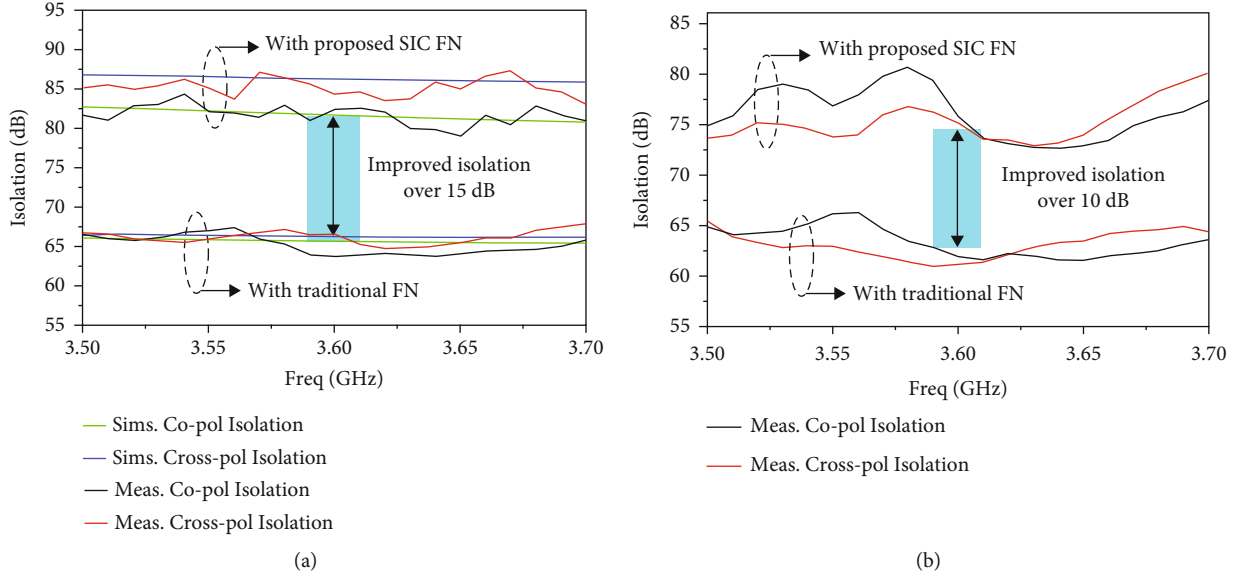
FIGURE 8: Copolarization and cross-polarization isolation between Tx and Rx ports with different FNs. (a) Measured in an anechoic chamber and simulated in HFSS. (b) Measured in a regular environment.
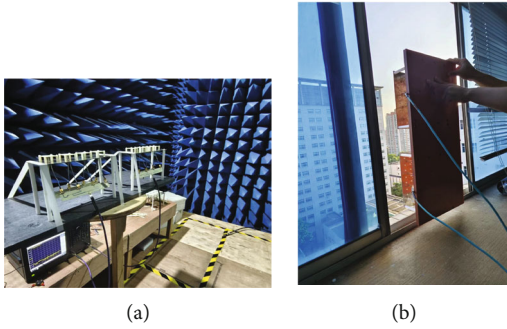

FIGURE 9: Photograph of the testing environment for the fabricated antenna. (a) In an anechoic chamber. (b) In a regular environment.

in the optimization procedure, $\omega_1 = [k_1, k_2, k_3, e_1, e_2, e_3]^T$ and $\omega_2 = [k_4, k_5, k_6, e_4, e_5, e_6]^T$ are set as optimization variables, which are associated with the FNs of Tx antennas and Rx antennas, respectively.

The input impedance of each T-junction is set to 50 ohms, so that the reflection coefficient of the FNs does not need to be considered in the optimization procedure, as the input impedance always matches 50 ohms. Then, the characteristic impedances Z_1-Z_6 in Figure 4 are given by

$$\begin{cases} Z_{2i-1} = 50\sqrt{\dfrac{k_i + 1}{k_i}}, & i = \{1, 2, 3\}. \\ Z_{2i} = 50\sqrt{k_i + 1} \end{cases} \quad (2)$$

Other fixed parameters shown in Figure 4 are given as follows: $Z_0 = 50\,\Omega$, $a_0 = 30°$, $a_1 = 270°$, and $a_2 = 140°$.

The S-parameter matrix corresponding to the topology in Figure 4 is easy to calculate. And the S-parameter matrix of the antenna array without FNs is obtained by the EM software HFSS. Based on the theory in [27], the S-parameter matrix
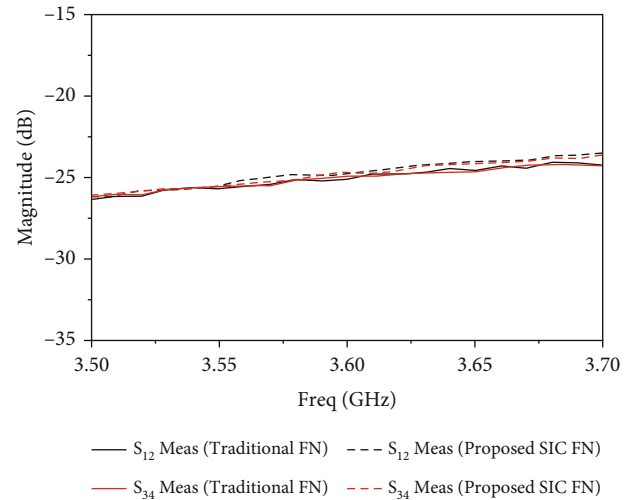

FIGURE 10: Measured $|S_{12}|$ and $|S_{34}|$ of the antenna with different FNs.

S^{total} of the antenna array with the FNs can be calculated, so the isolation between Tx and Rx ports can be obtained.

In addition, the radiation performance of each subarray is incorporated into the optimization procedure. Assume $F_0(0, 0)$ is the value of the standard realized gain radiation pattern in dB in the broadside direction, calculated by $\omega_0 = [1, 1, 1, 0, 0, 0]^T$. $F_m(0, 0)$ is the value of the realized gain radiation pattern of the mth subarray in dB in the broadside direction. To ensure good radiation performance, the maximum gain attenuation is set at 0.3 dB in the optimization procedure.

Finally, the objective function can be written as

$$\begin{cases} \min\left(\left[\left|S^{\text{total}}(i, j)\right|, i = 1, 2, j = 3, 4\right]_{\max}\right), \\ F_0(0, 0) - F_m(0, 0) \le 0.3\,\text{dB}, \quad m = 1, \cdots, 4. \end{cases} \quad (3)$$
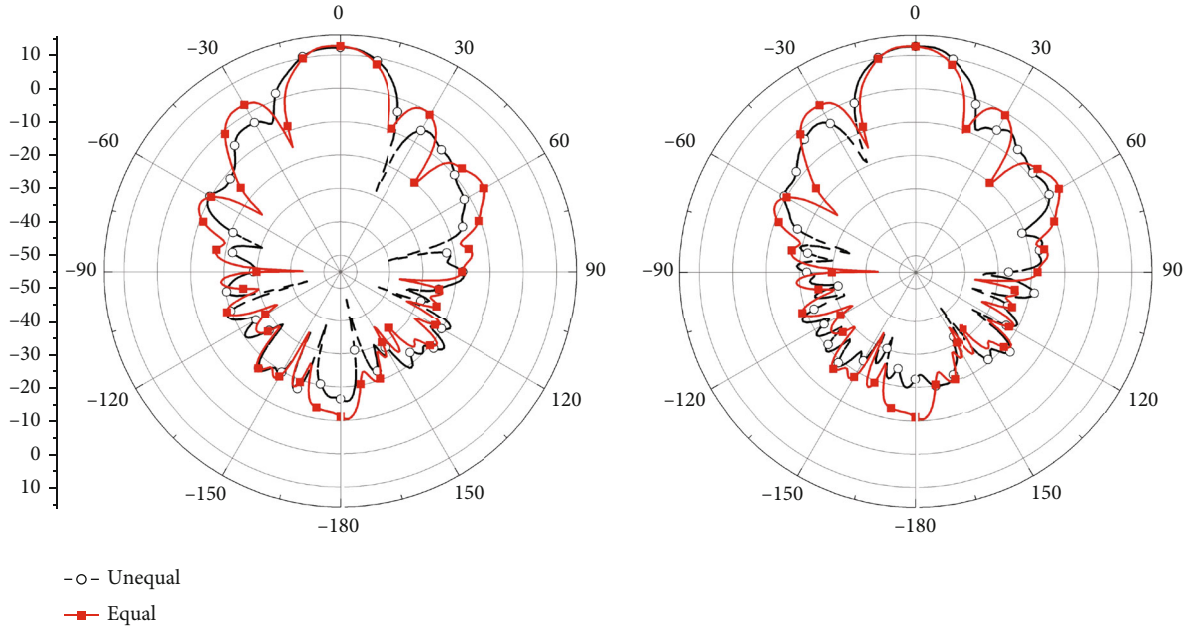
–◦– Unequal

–■– Equal

FIGURE 11: Measured radiation patterns of the Tx port and Rx port.

The design flowchart of the proposed SIC technique is summarized in Figure 5. As a result, the FNs, which can realize coupling cancellation and provide the desired radiation performance for the antenna array, can be obtained.

3. Numerical Result

In this section, to verify the performance and effectiveness of the proposed SIC technique, the above methodology was applied to design the FNs in Figure 3. A prototype was fabricated for measurement and comparison.

In the optimization procedure, the power ratio region is $0.25 < k < 4$, and the phase difference region is $0° < e < 360°$. The Python optimization procedure is repeated until a convergence criterion is met, and the optimal solution of the minimum isolation between the Tx and Rx ports is 82.7 dB at 3.6 GHz. Compared with the 66.2 dB isolation with the traditional FNs, which is computed using the variables $\omega_0 = [1, 1, 1, 0, 0, 0]^T$, the isolation is improved by 16.5 dB. The optimized results are listed in Table 2. Next, the optimized power ratios and phase differences can be converted to the impedance of the quarter-wavelength impedance transformer in the FNs using (2). Finally, the size of the optimized FNs based on a 0.76 mm RO4350B substrate ($\varepsilon_r = 3.48$ and $\tan \delta = 0.0037$) is shown in Figure 3. Table 2 shows the key dimensions of the SIC FNs.

The fabricated antenna and FNs are shown in Figure 6. The traditional FNs are also fabricated for comparison. To evaluate the performance of the antenna, we measured the reflection coefficient of each array element without FNs, which is below -15 dB (Figure 7(a)).After the antenna is connected to the FNs, the measured reflection coefficients of the antenna array with SIC FNs are the same level as that of the antenna array with traditional FNs, which are also below -15 dB (Figure 7(b)).
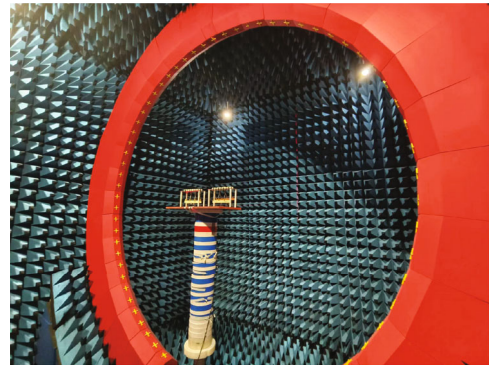

FIGURE 12: Measurement of the radiation patterns of the fabricated antenna array.

Figure 8 shows the simulation and measurement results for isolation. Among them, Figure 8(a) shows the results of measurements performed in an anechoic chamber (Figure 9(a)). At the measurement frequency point of 3.6 GHz, the copolarization isolation between Tx and Rx ports with the traditional FNs is about 66.8 dB. In contrast, the copolarization isolation with the proposed SIC FNs is about 82.3 dB, which improves the isolation by 15.5 dB. The isolation improvement of cross-polarization isolation between Tx and Rx ports is higher, about 17 dB. The above results, which agree well with the simulation, are due to the fact that the reflection in the anechoic chamber is very small. To assess the level of the impact in practice scenarios, in which the scatterers may appear, the isolation is measured in a regular environment, as shown in Figure 9(b). This environment simulates the scenario of the antenna acting as a base station on the base transceiver station tower. The measurement results are shown in Figure 8(b). It is seen that although

the isolation of the antenna with these two types of FNs decreased, the isolation with SIC FNs is still over 10 dB higher than that with traditional FNs. The degraded isolation is due to the environment scatterers, like the metal window frames. It should be noted that the antenna S-parameter matrix used in the design of the SIC FNs is calculated by HFSS on the premise that the antenna is not affected by environmental reflection. Therefore, the stronger the reflection in the practical scenario, the weaker the improvement of the isolation brought by the FNs.

Figure 10 shows the measured coupling results between the Tx ports or between the Rx ports. As seen, the measurement results are below -23 dB to meet engineering requirements.

Figure 11 displays a comparison of the measured radiation pattern at 3.6 GHz, which is measured in an anechoic chamber (Figure 12). The main beam of the antenna feeding with the SIC FNs broadens, and the sidelobe level is reduced. When feeding with the SIC FNs, the measured antenna gain is about 12.51 dBi at the Tx port and 12.90 dBi at the Rx port. And the gain feeding with the traditional FNs is 12.84 dBi for the Tx port and 13.03 dBi for the Rx port. There is a slight decrease in gain, roughly in line with the calculation result of the Python procedure, about 0.3 dB.

4. Conclusion

In this letter, a SIC technique for FNs is presented. The FNs with a specific size, which are designed by a Python optimization procedure, enable SIC. Therefore, the isolation can be improved. The proposed technique is verified by experiments. When the antenna with the SIC FNs is measured in an anechoic chamber, a significant 15 dB isolation improvement is obtained with a slight gain loss (about 0.3 dB) at 3.6 GHz. And when the antenna is in a practical scenario, the improvement in isolation is influenced by reflection from the surrounding environment. Therefore, the SIC technique has good potential in the scenario where the antenna is in an open environment, such as base station applications.

Data Availability

The datasets used or analyzed during the current study are available from the corresponding author on reasonable request.

Conflicts of Interest

No potential conflict of interest was reported by the authors.

References

[1] K. E. Kolodziej, B. T. Perry, and J. S. Herd, "In-band full-duplex technology: techniques and systems survey," *IEEE Transactions on Microwave Theory and Techniques*, vol. 67, no. 7, pp. 3025–3041, 2019.

[2] S. Hong, J. Brand, J. Choi et al., "Applications of self-interference cancellation in 5G and beyond," *IEEE Communications Magazine*, vol. 52, no. 2, pp. 114–121, 2014.

[3] M. Tsunezawa, K. Takahashi, N. Honma, K. Murata, and K. Nishimori, "Antenna arrangement suitable for full-duplex MIMO," *IEEE Transactions on Antennas and Propagation*, vol. 65, no. 6, pp. 2966–2974, 2017.

[4] S. Masuyama, Y. Yamamoto, N. Honma, K. Murata, Q. Yuan, and Q. Chen, "Analog interference suppression using end-fire arrays and 180-degree hybrids for full-duplex MIMO," in *2019 Asia-Pacific microwave conference (APMC 2019), F1-7*, pp. 1290–1292, 2019.

[5] K. L. Scherer, S. J. Watt, E. A. Alwan et al., "Simultaneous transmit and receive system architecture with four stages of cancellation," in *2015 IEEE International Symposium on Antennas and Propagation & USNC/URSI National Radio Science Meeting*, pp. 520-521, Vancouver, BC, Canada, 2015.

[6] G. S. Shiroma, R. Y. Miyamoto, and W. A. Shiroma, "A full-duplex dual-frequency self-steering array using phase detection and phase shifting," *IEEE transactions on Microwave Theory and Techniques*, vol. 54, no. 1, pp. 128–134, 2006.

[7] H. Nawaz, N. Ahmad, and J. Aslam, "A unidirectional, printed antenna with high interport isolation over wider bandwidth for 2.4 GHz full duplex applications," *IEEE Transactions on Antennas and Propagation*, vol. 69, no. 11, pp. 7183–7191, 2021.

[8] F. Yang and Y. Rahmat-Samii, "Microstrip antennas integrated with electromagnetic band-gap (EBG) structures: a low mutual coupling design for array applications," *IEEE Transactions on Antennas and Propagation*, vol. 51, no. 10, pp. 2936–2946, 2003.

[9] M. G. N. Alsath, M. Kanagasabai, and B. Balasubramanian, "Implementation of slotted meander-line resonators for isolation enhancement in microstrip patch antenna arrays," *IEEE Antennas and Wireless Propagation Letters*, vol. 12, pp. 15–18, 2013.

[10] L. Wang, Y.-X. Guo, and W.-X. Sheng, "Wideband high-gain 60-GHz LTCC L-probe patch antenna array with a soft surface," *IEEE Transactions on Antennas and Propagation*, vol. 61, no. 4, pp. 1802–1809, 2013.

[11] H. Qi, X. Yin, L. Liu, Y. Rong, and H. Qian, "Improving isolation between closely spaced patch antennas using interdigital lines," *IEEE Antennas and Wireless Propagation Letters*, vol. 15, pp. 286–289, 2016.

[12] G. Zhai, Z. N. Chen, and X. Qing, "Enhanced isolation of a closely spaced four-element MIMO antenna system using metamaterial mushroom," *IEEE Transactions on Antennas and Propagation*, vol. 63, no. 8, pp. 3362–3370, 2015.

[13] K. Kumari, M. Saikia, R. K. Jaiswal, S. Malik, and K. V. Srivastava, "A compact, low-profile shorted $TM_{1/2,0}$ mode planar copolarized microstrip antenna for full-duplex systems," *IEEE Antennas and Wireless Propagation Letters*, vol. 21, no. 9, pp. 1887–1891, 2022.

[14] X. Wang, W. Che, W. Yang, W. Feng, and L. Gu, "Self-interference cancellation antenna using auxiliary port reflection for full-duplex application," *IEEE Antennas and Wireless Propagation Letters*, vol. 16, pp. 2873–2876, 2017.

[15] R. Xia, S. Qu, P. Li, Q. Jiang, and Z. Nie, "An efficient decoupling feeding network for microstrip antenna array," *IEEE Antennas and Wireless Propagation Letters*, vol. 14, pp. 871–874, 2015.

[16] A. Diallo, C. Luxey, P. L. Thuc, R. Staraj, and G. Kossiavas, "Study and reduction of the mutual coupling between two mobile phone PIFAs operating in the DCS1800 and UMTS

bands," *IEEE Transactions on Antennas and Propagation*, vol. 54, no. 11, pp. 3063–3074, 2006.

[17] D. Nie, B. M. Hochwald, and E. Stauffer, "Systematic design of large-scale multiport decoupling networks," *IEEE Transactions on Circuits and Systems I: Regular Papers*, vol. 61, no. 7, pp. 2172–2181, 2014.

[18] Y. Chen, C. Hua, Y. Lu, and J. Huang, "A bandwidth-enhanced tunable decoupling method for compact mobile terminal antennas," *IEEE Transactions on Antennas and Propagation*, vol. 70, no. 8, pp. 6455–6468, 2022.

[19] K.-L. Wu, C. Wei, X. Mei, and Z.-Y. Zhang, "Array-antenna decoupling surface," *IEEE Transactions on Antennas and Propagation*, vol. 65, no. 12, pp. 6728–6738, 2017.

[20] J. Guo, F. Liu, L. Zhao, G.-L. Huang, W. Lin, and Y. Yin, "Partial reflective decoupling superstrate for dual-polarized antennas application considering power combining effects," *IEEE Transactions on Antennas and Propagation*, vol. 70, no. 10, pp. 9855–9860, 2022.

[21] Y.-M. Zhang and J.-L. Li, "Differential-series-fed dual-polarized traveling-wave array for full-duplex applications," *IEEE Transactions on Antennas and Propagation*, vol. 68, no. 5, pp. 4097–4102, 2020.

[22] D. Wojcik, M. Surma, A. Noga, and M. Magnuski, "Design of dual-polarized MIMO linear antenna arrays with increased port-to-port isolation," in *2016 21st International Conference on Microwave, Radar and Wireless Communications (MIKON)*, pp. 1–3, Krakow, Poland, 2016.

[23] D. Wojcik, M. Surma, A. Noga, and M. Magnuski, "High port-to-port isolation dual-polarized antenna array dedicated for full-duplex base stations," *IEEE Antennas and Wireless Propagation Letters*, vol. 19, no. 7, pp. 1098–1102, 2020.

[24] M. A. Elmansouri, L. B. Boskovic, and D. S. Filipovic, "Compact wideband dual-polarized in-band full-duplex antenna subsystem," *IEEE Transactions on Antennas and Propagation*, vol. 69, no. 11, pp. 7166–7172, 2021.

[25] P. Xingdong, H. Wei, Y. Tianyang, and L. Linsheng, "Design and implementation of an active multibeam antenna system with 64 RF channels and 256 antenna elements for massive MIMO application in 5G wireless communications," *China Communications*, vol. 11, no. 11, pp. 16–23, 2014.

[26] L. Wu, R. Li, Y. Qin, and Y. Cui, "Bandwidth-enhanced broadband dual-polarized antennas for 2G/3G/4G and IMT services," *IEEE Antennas and Wireless Propagation Letters*, vol. 17, no. 9, pp. 1702–1706, 2018.

[27] G. Simpson, "A generalized n-port cascade connection," in *1981 IEEE MTT-S International Microwave Symposium Digest*, pp. 507–509, Los Angeles, CA, USA, 1981.

[28] Q.-X. Chu, D.-L. Wen, and Y. Luo, "A broadband ±45° dual-polarized antenna with Y-shaped feeding lines," *IEEE Transactions on Antennas and Propagation*, vol. 63, no. 2, pp. 483–490, 2015.